LA-3417-MS

LOS ALAMOS SCIENTIFIC LABORATORY
of the
University of California
LOS ALAMOS • NEW MEXICO

Air Fluorescence Excited by High-Altitude Nuclear Explosions

CIC-14 REPORT COLLECTION
REPRODUCTION
COPY

UNITED STATES
ATOMIC ENERGY COMMISSION
CONTRACT W-7405-ENG. 36

LA-3417-MS
Special Distribution

LOS ALAMOS SCIENTIFIC LABORATORY
of the
University of California
LOS ALAMOS • NEW MEXICO

Report written: April 1965
Report distributed: January 5, 1966

Air Fluorescence Excited by High-Altitude Nuclear Explosions

by
Herman Hoerlin

ABSTRACT

Nuclear explosions in or above the upper atmosphere give rise to strong excitation of air constituents. Of the total energy released in the explosion, approximately 70% appears as x rays; and in the absorption process as much as 5% of this energy is converted promptly into visible and near-visible emission from the N_2^+ first negative and the N_2 second and first positive systems. The precise character of this radiation is dependent on total dose and altitude of delivery. If the excited volume is optically thick, the radiation transport is governed by self-absorption, quenching, charge exchange, and recombination processes. These must be considered in spectroscopic analysis. The kinetic energy residing in fast-moving bomb debris (initial velocity $\sim 10^8$ cm/sec) and in fission beta particles may amount to 25% of the yield, and the stopping process will lead to additional excitation and to phenomenologically interesting displays. Thus the motion of debris from "Starfish" (1.5 Mt at 400 km) and the interaction of the debris with the geomagnetic field and the atmosphere could be traced through characteristic emission from atomic oxygen and nitrogen. Formation of an elongated plasma bubble, jetting of debris to altitudes of 2000 km, and subsequent relaxation of the disturbed field were observed.

ACKNOWLEDGMENTS

This summary article is the slightly revised version of an invited paper presented at the Spring Meeting of the Optical Society of America in Dallas, Texas, April 2, 1965. It is based on the work of many. Besides those mentioned in the text, the field contributions by Milton Peek, Donald R. Westervelt, Robert Kiehn, and Sidney Stone must be acknowledged as well as photographic contributions by Roy Stone, Winfred Headdy, and William Regan, all of LASL, and by members of the EG&G teams. The observational field program was only made possible through the continuous active support of William Ogle, Scientific Deputy of Joint Task Force 8.

TABLE OF CONTENTS

LIST OF ILLUSTRATIONS

LIST OF ILLUSTRATIONS (continued)

INTRODUCTION

Nuclear explosions in the upper atmosphere and in near space have been conducted primarily for military purposes. However, besides producing effects of importance to national defense, such events have generated rich returns of scientific information in many fields.

The widespread geophysical effects accompanying a high-altitude explosion exhibit great similarity with natural events in the upper atmosphere, which cannot be duplicated in the laboratory. Indeed the multitude of phenomena produced by one known source, the interaction of various types of energy with the atmosphere and the earth's magnetic field, is--though complicated--highly informative, striking, and at times very spectacular.

Before coming to the main subject of this presentation, the review of such interactions, it will be instructive to see two beautiful, almost classroom, demonstrations of physical phenomena occurring at high altitudes.

The first is the detonation of "Starfish," a 1.5-Mt device, exploded at an altitude of 400 km above Johnston Island near midnight of July 9, 1962. From the 10,000-ft-high top of the extinct volcano Haleakala on Maui Island in the Hawaiian chain, one sees at a distance of about 1500 km two distinct phases of the explosion (Fig. 1):

a) The birth of a tiny shortlived artificial star which radiates brightly for about 1 msec, the light being emitted by the expanding bomb debris. In the cooling process part of the internal energy of the hot bomb material is converted into visible light.

b) The vast bright air glow produced by the absorption of the bomb-produced x radiation in a large volume of the atmosphere. In the collision process, the x rays and their photoelectrons excite characteristic air fluorescence, which illuminates the sky. The physics of this air fluorescence will be the first major subject of this paper.

Another demonstration (Fig. 2) shows the complicated phenomena occurring as a consequence of the detonation of a medium-yield device, also above Johnston Island, but at a lower altitude than Starfish. Here we observe the fireball, seconds after the explosion, from a high-flying aircraft, looking from east to west perpendicular to the magnetic meridian. The bright elongated plasma bubble, a mixture of hot air and debris, has already risen above the burst point. The magnetic field inside the bubble is "frozen" into the plasma and stretched upwards. The beta particles originating in the fission products are spiralling along these stretched field lines to the edge of the bubble where they change direction following now the undisturbed field, at its normal dip of 30° to the horizontal, until they are stopped in the denser atmosphere. This demonstration of the interaction of a plasma with the geomagnetic field and of the discrete motion of particles, first in the deformed and then in the natural field, is quite impressive. A more precise though still qualitative description of another interaction of this type will be the second major theme of this report.

In addition one observes in Fig. 2 the interaction of the upward-moving shock with atomic species dominant at higher altitudes which emit the red glow. The downward-moving front collides with the molecular species of the lower atmosphere and contributes to the emission of the green glow which is due to the nitrogen afterglow reaction

$NO + O \rightarrow NO_2 + h\nu$.

I. AIR FLUORESCENCE PRODUCED BY X RAYS

The air glow demonstrated in the form of the bright sky light in Fig. 1 has been the subject of extensive studies. It has great similarities with the often brilliant emission from natural aurorae. Both are produced mainly by electrons, in the first case by the photoelectrons ejected from the air molecules as a consequence of the absorption of x-ray photons, and in the second case by electrons originating in the solar atmosphere.

Essentially, in our case, the photoelectrons excite the various electronic states of the nitrogen molecule and the singly ionized molecular nitrogen ion. Characteristic emission occurs, a large fraction of which can be observed in the visible and near visible wavelength regions. These are mainly the 2P, second positive, and 1P, first positive, systems of N_2 and the 1N, first negative system of N_2^+, which are shown in the energy level diagram of Fig. 3. Emission from other systems, such as from the singlets and the "forbidden" transitions in the Vegard-Kaplan bands, occur in the invisible ultraviolet part of the spectrum.

It is of interest to study the nature of the excitation process or, in other words, the brightness of the excited mass of air molecules under the conditions dictated by the high-altitude events. The volume of air exposed to the x rays emitted by the device is very large, in contrast to the very small volumes one can use in the laboratory.

In laboratory experiments nitrogen gas of low density has been bombarded with electrons of comparable energy by A. L. Stewart in England and Sheridan, Oldenberg, and Carleton in this country. Eliminating secondary excitation processes, cross sections have been determined for the most prominent emission, the (0,0) transition of the first negative system of N_2^+ at 3914 $\mathring{A}$, which correspond to a fluorescence efficiency of 0.2%; i.e. 0.2 of 1% of the corresponding electron energy deposited is reemitted in this one band. Also in the laboratory under

somewhat different experimental conditions, not excluding secondary processes, Hartman and the author found for this band a conversion efficiency of 0.35%.

During the 1958 and 1962 high-altitude test series, LASL physicists conducted a whole series of experiments in which the air fluorescence was observed spectroscopically, time integrated and time resolved along many lines of sight, ground-based from Johnston Island and from the top of Mt. Haleakala on Maui Island, as well as from a high-flying instrumented KC-135 aircraft. These lines of sight avoided the warhead itself and bypassed the burst location at varying distances. Thus the light originated in columns of air dosed--i.e. exposed to x rays--to varying degrees. Close in to the source the dose was high, producing promptly as much as 2×10^{13} N_2^+ ions/cc. At the largest distance and for the lowest source strength, the prompt ion concentration was 2×10^8, still a rather high number. The time history of the total emission from a column depends on many parameters; besides source strength and altitude, factors such as distance of the line of sight from the burst, geometrical details, and the resulting number of radiating ions play important roles. Perhaps better expressed, the precise physical state of the column of air at the times preceding the arrival of the photons at the sensor, i.e. while in transit, determines their intensity. For example, photons produced at a relatively low altitude will arrive at the sensor first; other photons generated at a higher altitude, say at the altitude of maximum energy deposition, will arrive later after passing through previously dosed air; and, finally, photons generated at still higher altitudes must pass through a long column of heavily dosed air. During passage through this air the light undergoes many resonance scattering processes, with a consequent redistribution of the energy among other transitions in the system. For instance a 3914 Å (0,0) photon after reabsorption by N_2^+ in the ground state with a given population of the vibrational levels has a 30% probability to be reemitted as a 4278 Å (0,1) photon and a roughly 10% probability to appear as a 4709 Å (0,2)

photon. Since the probability for reabsorption of the longer wavelength photons is smaller, the relative intensities of the transitions seen by the sensor may differ from "normal," i.e. from the distribution at generation time. Thus in the case of high dose the observed 3914 Å intensity should be drastically decreased and the long wavelength transitions enhanced.

This is what actually happened in practically all high-altitude events of the 1958 and 1962 test series. As a typical example the "normal" relative intensities obtained in small volumes of air in the laboratory are shown in Fig. 4 together with the "abnormal" relative intensities seen in the large volume of the highly dosed atmosphere of the Starfish detonation. The actual Starfish spectrograms from which these numbers were taken are shown in Fig. 5.

If one were tempted to derive from measurements of this sort the fluorescence efficiency of air for a particular band, say for the 3914 Å band which is normally the strongest, one would encounter serious difficulties and, indeed, one does. In such derivations one must compute the energy deposited along a given line of sight using the characteristics of the x-ray spectrum of the source and the absorption coefficients of air; one then integrates the light output of the column as function of time using a nominal conversion efficiency factor. Comparing the observed brightness values with the computed numbers, the apparent efficiency is obtained. This was done for a large number of observations taken on the Starfish, Kingfish, Bluegill, and Teak events; the results for the 3914 Å band are plotted in Fig. 6 as a function of the prompt N_2^+ density per square centimeter integrated along the line of sight column. The trend of this graph, an apparent decrease of the efficiency with increasing ion density, is due to the redistribution process described earlier. Resonance scattering, i.e. self-absorption, shifts energy away from the 3914 Å (0,0) transition to longer wavelengths. Clearly further analysis had to be done to find the true source function.

In order to gain, first, a better qualitative understanding of this imprisonment process, Jahoda, Mullaney, Stone, and the author designed a relatively simple model to calculate the effects of increasing ion density using the Monte Carlo method. Briefly, a given number of N_2^+ 1N photons (0,0; 0,1; 0,2; and 0,3 transitions) was generated with normal intensity distribution in the center of a large cylinder of air and emitted at random. The subsequent walk of the photons is governed by the effective absorption cross sections, the fractional populations of the ground state, and the Einstein coefficients of the various transitions. For a series of constant ion densities the number and "color" of photons emerging from the bottom of the cylinder was computed (Fig. 7). Qualitatively this model was most useful; a relative intensity distribution such as the one seen in the Starfish spectrum (Figs. 4 and 5) would occur for 10^{14} ions/cm^2 in the column. In reality, however, the number of ions produced promptly along the Starfish line of sight was about three magnitudes larger.

Consequently, calculations of this general nature had to be refined to do justice to the actual conditions, the exponential nature of the atmosphere, the travel time of the photons, their residence time in the excited states, Doppler broadening, and their exit angles. N_2^+ is also continuously removed either by charge exchange with O_2 or by dissociative recombinations. For the purpose of analyzing the raw field data shown in Fig. 6, E. Bennett wrote a new Monte Carlo type "High Altitude Resonance Absorption Code, HARAC" which was designed to reproduce field conditions and to calculate apparent surface brightness for the four major bands of the first negative system. The basic parameters used are tabulated in Fig. 8. As a result of these calculations the wide spread of the observed efficiencies, from 0.007 to 0.9%, has been narrowed to 0.6 to 1.5% with a most probable value of 1% for 3914 Å.

This number is considerably higher than the laboratory data quoted earlier; the reasons for this discrepancy remain to be resolved. The total efficiency for the three main visible and near-visible band

systems comes to 5%, also a rather high value.

The observations of the high-altitude air fluorescence during the 1958 test series led to an interesting byproduct, namely to the conception and the design, by D. R. Westervelt and the author, of a ground-based detection system for nuclear explosions in space. The system was subsequently reviewed by the U. S. delegation to the Geneva Test Ban negotiations in 1959 and proposed to become part of an international detection network. It was technically accepted by all participants.

Essentially the discrete emission of the powerful 3914 Å band can be observed in bright daylight for relatively small and distant sources by means of all-sky optics, narrow bandpass interference filters (which transmit 3914 Å, but eliminate almost all sky light), and sensitive photodetectors. A self-explanatory schematic view of the system, its nominal detection range, and a typical signal shape are shown in Fig. 9. The fluorescence efficiency of the 3914 Å band enters dominantly in the constant of the range formula, besides the optical, photoelectric, and electronic components of the system.

II. BOMB DEBRIS EXCITED AIR FLUORESCENCE

OBSERVATIONS OF THE MOTION OF DEBRIS

It was stated earlier that an explosion such as "Starfish" releases approximately 70% of its energy in the form of x rays which travel to distant points. A much smaller fraction of the yield appears in the form of internal energy of the highly ionized bomb debris, part of which is emitted as visible light in the course of the cooling process (the "star" of Fig. 1). A third sizeable fraction, perhaps 20 to 25% of the prompt yield, shows up as kinetic energy of the rapidly expanding bomb debris. This section reviews the interaction of this energy with the environment.

Fortunately the debris motion manifests itself over a considerable length of time by emission of light. The emission processes are more

complex than those described in the preceding section. Part of the light is due to recombination radiation in the debris material itself, part is caused by the collisions of the heavy and fast-moving debris ions with air constituents; light is also produced by the impact of the hydromagnetic shock wave on the atmosphere; finally the stopping of beta radiation from the decaying fission products leads to additional excitation of air.

No attempt will be made in this context to describe these processes in every detail. We confine ourselves to the analysis of the motion of the debris on the basis of the photographic evidence which permits interpretation of dimensions, color, and brightness as functions of time in terms of mass motion and thus leads to a good qualitative understanding of the complex hydromagnetic phenomena which govern the many phases of the explosion.

The highly ionized debris particles travel at first with velocities of the order of 10^8 cm/sec seemingly unimpeded through very thin but partially ionized air. Eventually they are slowed down by collisions but also by interaction with the environment through the geomagnetic field. The debris plasma moving in the magnetic field induces electric currents. The currents in turn produce forces which tend to change the state of motion of the plasma, transferring the initial movement to the surrounding gas, thus producing an Alfvén wave, i.e. a magnetohydrodynamic shock. This shock too is gradually slowed down by picking up increasing amounts of air ions. Because of the inhomogeneities of the atmosphere, of the ion densities within the atmosphere, and of the geomagnetic field, those motions are more complicated than those in the following simple but illustrative example.

If in absence of air a bomb plasma of 1 kt = 4×10^{19} ergs kinetic energy were generated in a homogeneous magnetic field of B = 0.5 gauss strength, a "magnetic bubble" of about 100 km radius in the direction perpendicular to the field lines would be formed. The energy content of the field is $B^2/8\pi$ ergs/cm^3, the field pressure $B^2/8\pi$ dyne/cm^2.

Along the field lines, through the necks of the "bottle" where the field exerts no pressure, the plasma would move unimpeded.

In the case of the Starfish explosion, the energies and therefore the dimensions involved are much larger, air is present, and the inhomogeneities mentioned earlier play a strong role. Four hundred kilometers above Johnston Island (location 16.5° N geographic, 14.6° geomagnetic) the field is diverging in the upward direction toward the equator and converging in the northerly downward direction. Furthermore, the radial field strength, radial from the center of the earth's dipole, decreases with R^{-3}. Thus one would expect the formation of a very asymmetrical bubble, perhaps similar to that shown in Fig. 10. One would also expect to see beta rays and debris escape through the "necks" toward north and south. Finally, it was predicted by Longmire that conditions would arise which favor formation of Taylor and flute instabilities--similar to those that make magnetic containment of thermonuclear reactions in the laboratory so very difficult--which in turn enhance motion of plasma across the field lines and partial venting to very high altitudes and into near space.

All these phenomena were documented from photographic observation stations on Johnston Island, Christmas Island, Haleakala, and in a high-flying aircraft. The geographies of these locations and the approximate fields of view of cameras are shown in Fig. 11.

Good evidence for the bubble formation exists by looking from Maui, Haleakala, almost straight west (WSW). In order to be able to visualize the delineation of the magnetic lines of force for a given view, A. Petschek wrote a code which permits the projection of field lines into the field of view of any camera. Figure 12 shows such a projection for the view from Haleakala. A corresponding photograph taken a fraction of a second after zero time is shown in Fig. 13. The bright spot near the center of the frame is not light emitted by the bomb debris, the disassembled material having travelled far at this time; it is rather the light from the hot Thor booster. The booster was separated from the

warhead long before explosion time but subsequently heated by collisions with debris. The oval bright green glow delineates at this time the spatial distribution of the debris, i.e. the "bubble" and the hydromagnetic shock front, light emission being predominantly due to excited atomic oxygen, the green line. To the north one sees, dipping about 30° to the horizontal, a yellow glow produced by the collisions of the escaping debris, escaping through the bottle neck, and of the fission beta rays with the lower, denser atmosphere. The yellow color in this area does not quite represent the true source color because of strong atmospheric absorption of the blue components in the long atmospheric path near the horizon.

Moving now to Christmas Island and looking northwest, the burst location appears almost exactly at the horizon. The projections of the undisturbed field lines are shown in Fig. 14, and the brilliant color display of the debris in a photograph taken at + 60 sec is seen in Fig. 15. A comparison of the field projections and the auroral display suggests that a large fraction of the debris is moving at first tangentially to a line perhaps 200 km above the burst, not following the bend of the field and indeed crossing the field lines in a noticeably diverging manner. That the debris were coasting to great heights became even more evident when viewing the same display from the aircraft looking south. The airplane was flying 1040 km NNE from the burst. Here we see, also at about + 60 sec (Fig. 16), the debris motion in the violently distorted field, part of the debris going north, other debris south. Almost 3 min later the strongly disturbed field has relaxed, i.e. it is almost normal again, and the remaining debris material, mixed with excited air constituents, is well aligned with the field. This is shown in Fig. 17 which should be compared with the field line and star projections of Fig. 18. Note the star images in Fig. 17 are slightly blurred because of airplane motion during the 3-sec exposure duration.

Spectroscopic evidence like the sample reproduced in Fig. 19 shows that the yellow glow in Figs. 16 and 17 is mainly due to the green and

red "auroral" oxygen lines at 5577 and 6300 Å, which in natural aurorae are excited mainly by auroral beta rays and photons. The brilliant red color in the surrounding space is the afterglow from the forbidden red oxygen lines at 6300 and 6364 Å which were excited in this case by the magnetohydrodynamic shock that has separated earlier from the debris.

Finally, it is interesting to note that these photographic observations of the debris motion to altitudes of at least 2000 km above the equator (Figs. 17 and 18) are qualitatively in agreement with Van Allen's measurements in the Injun satellite and also those of Brown and Hess in Telstar I. Detectors in these satellites mapped the artificial radiation belts produced by the beta particles emitted from the fission products in the jetting debris. From the ground air fluorescence was seen as far south as Christchurch in New Zealand; field lines terminating in New Zealand cross the equator at altitudes of many thousand kilometers.

A more detailed and quantitative analysis of these phenomena is currently being conducted by J. Zinn and others. It will be presented elsewhere.

Fig. 1. The Starfish explosion at midnight of July 9, 1962, from Mt. Haleakala. Camera shutter was opened before zero time and closed promptly at explosion time. Bright spot in cloud, upper right, is moon.

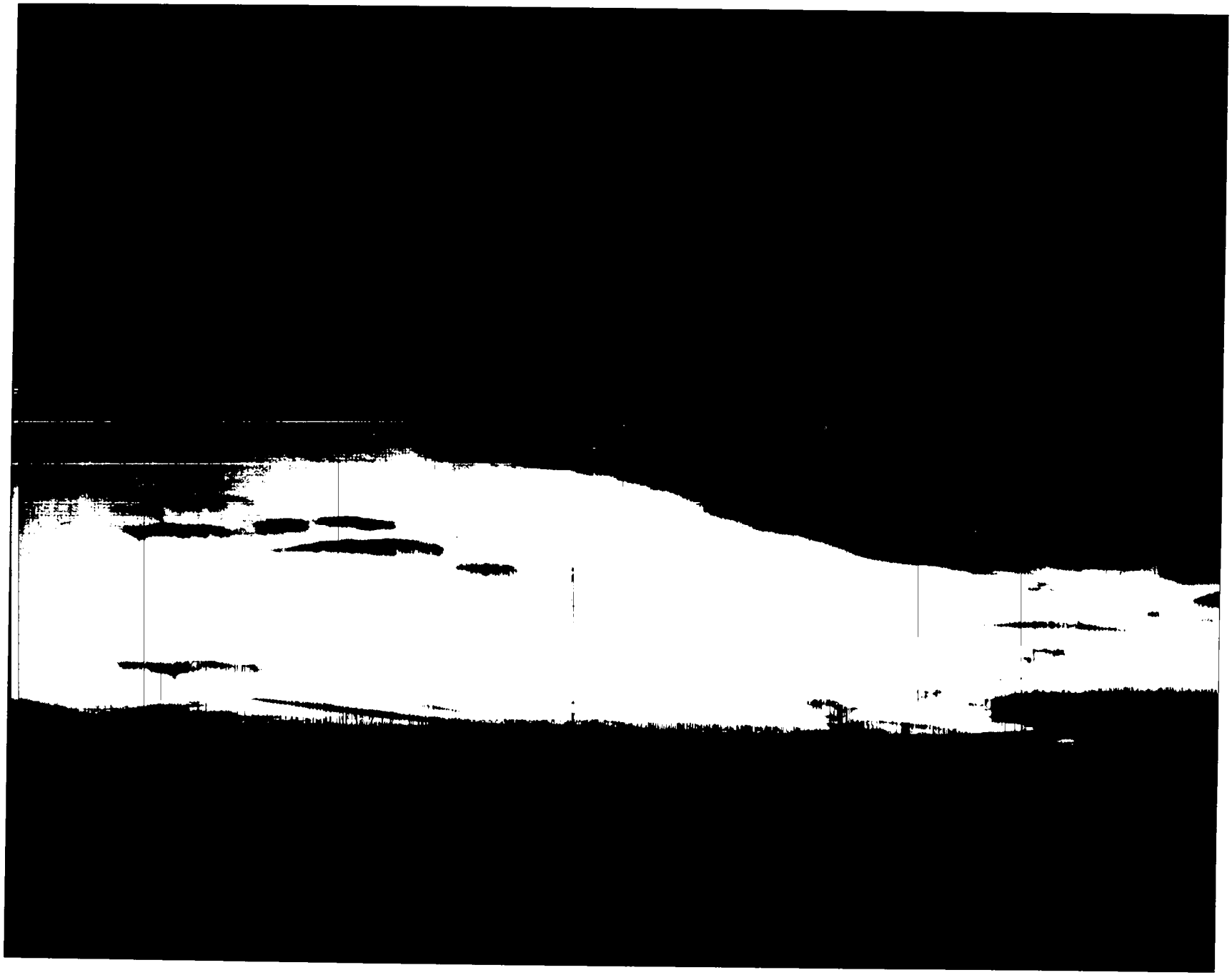

Fig. 2. Fireball produced by a medium-yield device detonated above Johnston Island. Wind-blown trail below is from instrumented companion rocket.

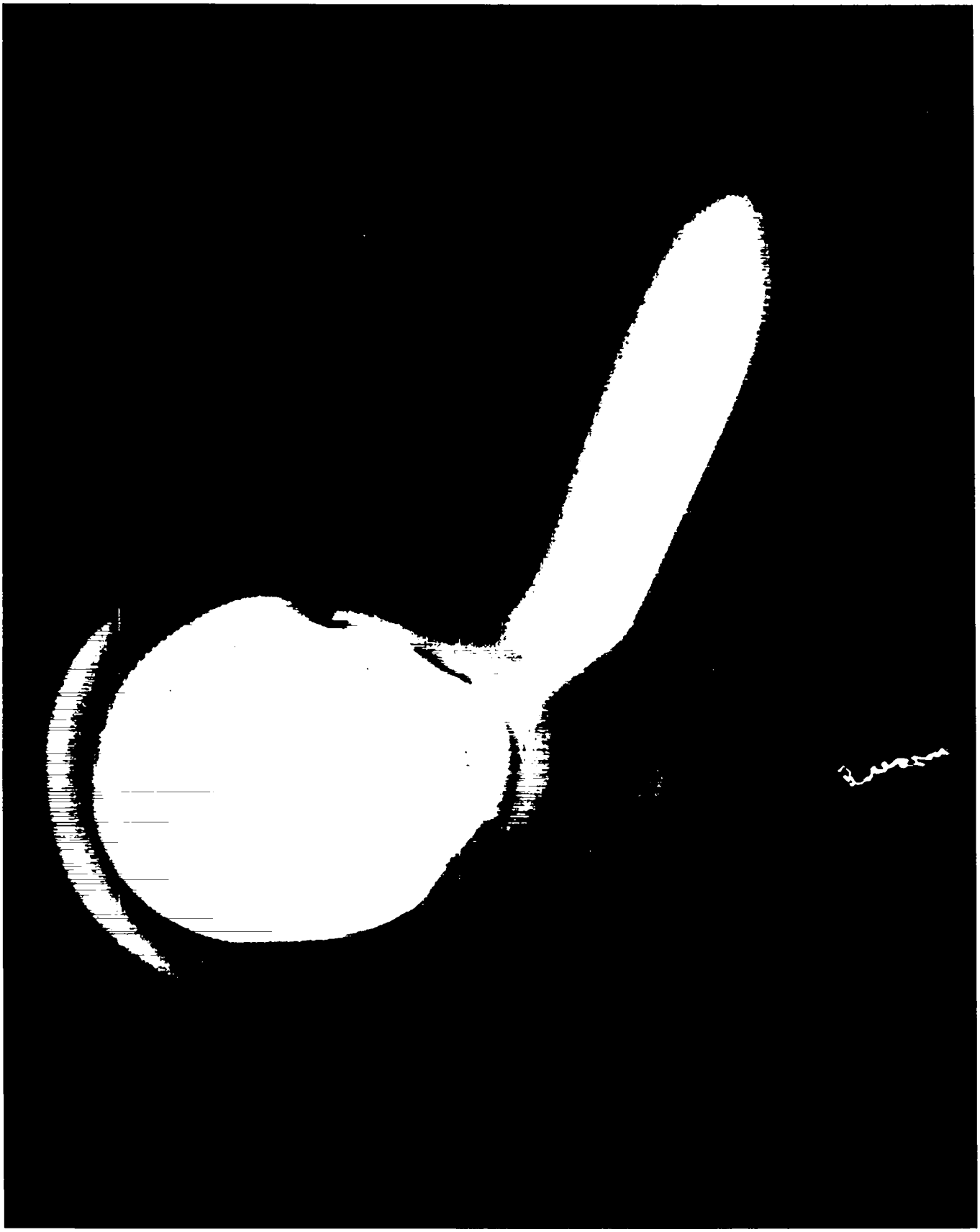

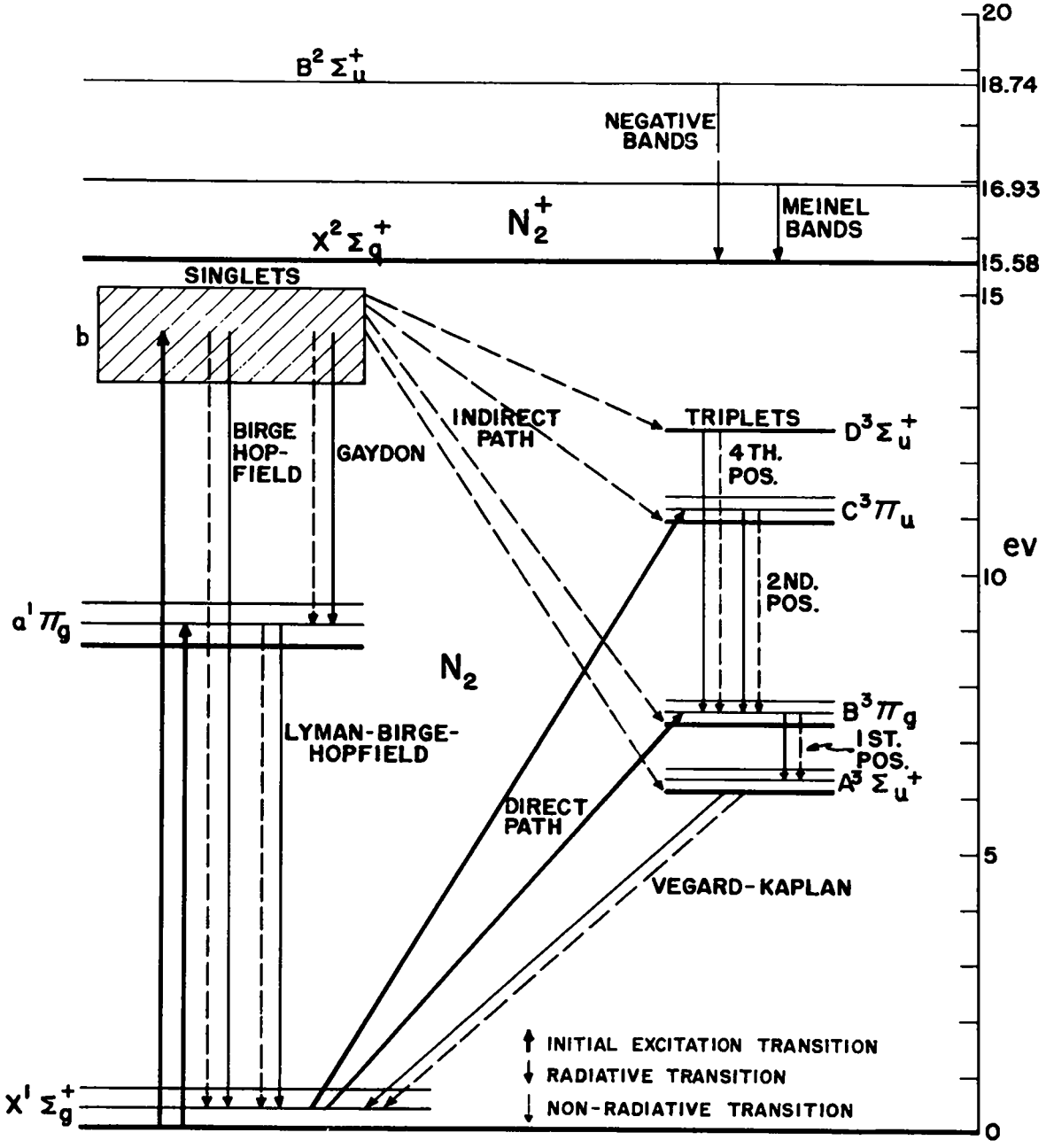

Fig. 3. Energy level diagram of molecular nitrogen, N_2 and N_2^+.

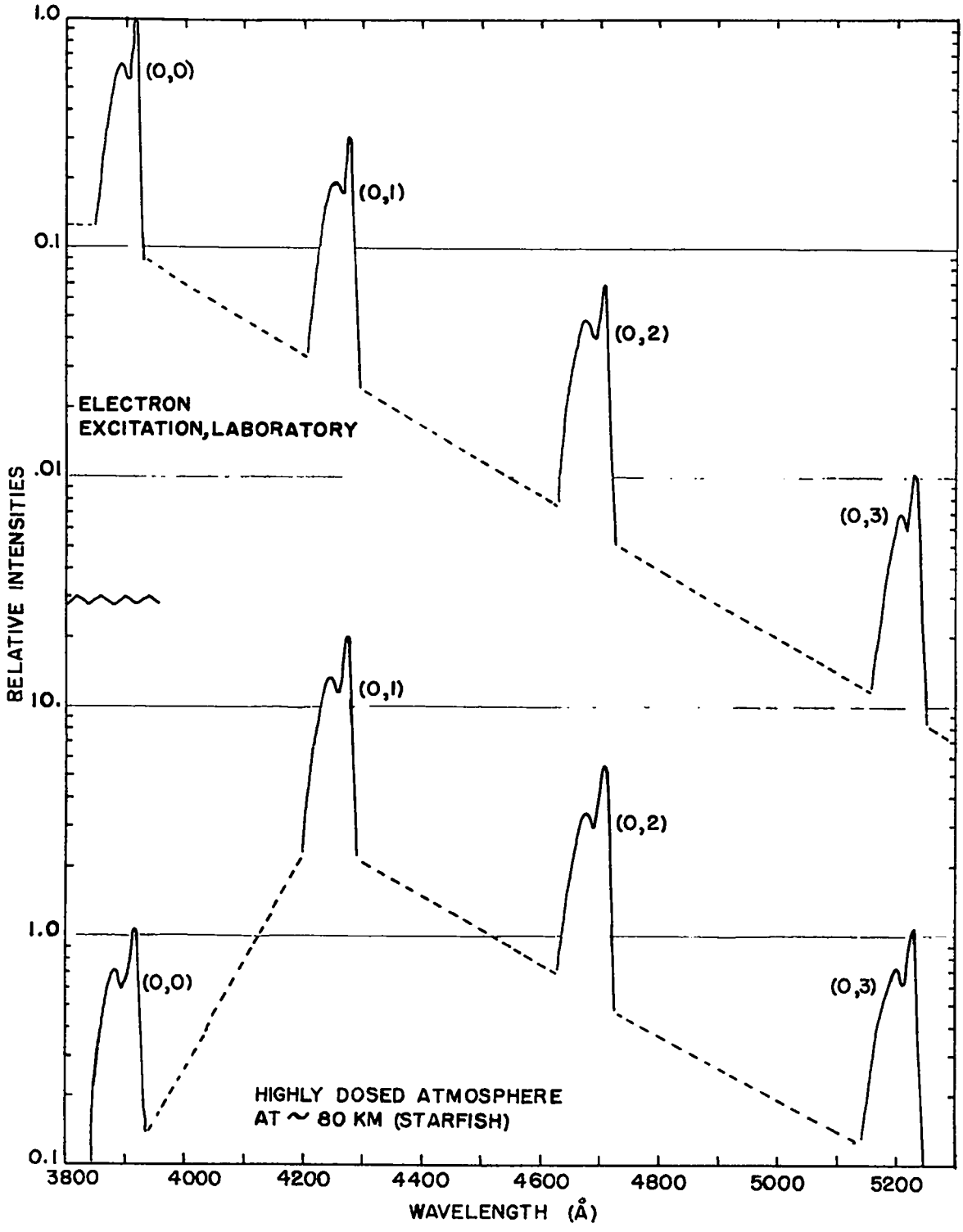

Fig. 4. N_2^+ first negative system relative intensities, schematic.

Fig. 5. 3300 - 5100 Å.

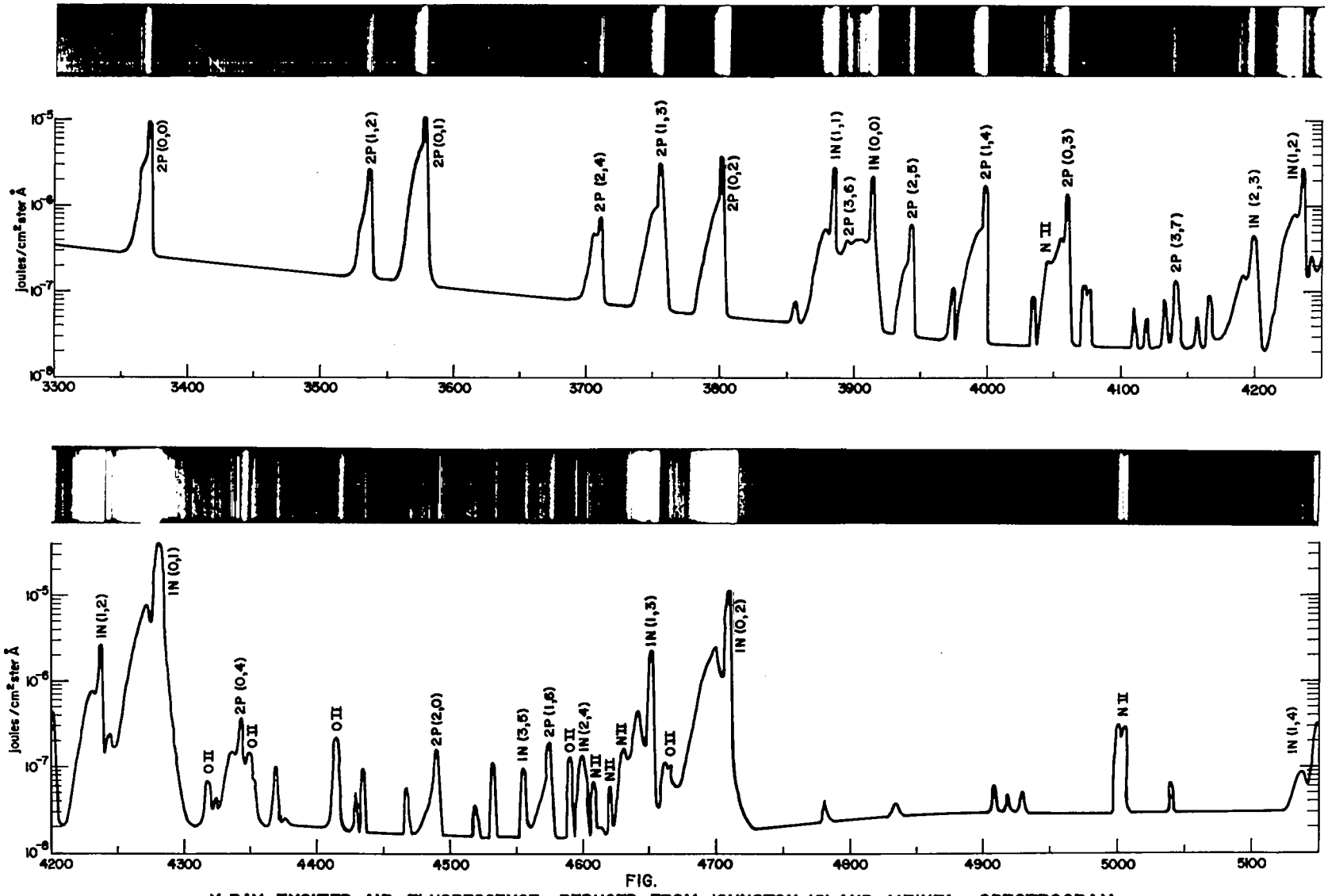

FIG.

X-RAY EXCITED AIR FLUORESCENCE. REDUCED FROM JOHNSTON ISLAND MEINEL SPECTROGRAM
LINE OF SIGHT 20° SOUTH OF STARFISH, EXPOSURE 0-76 μSEC.

Fig. 5. (Continued) 5100 - 6900 Å.

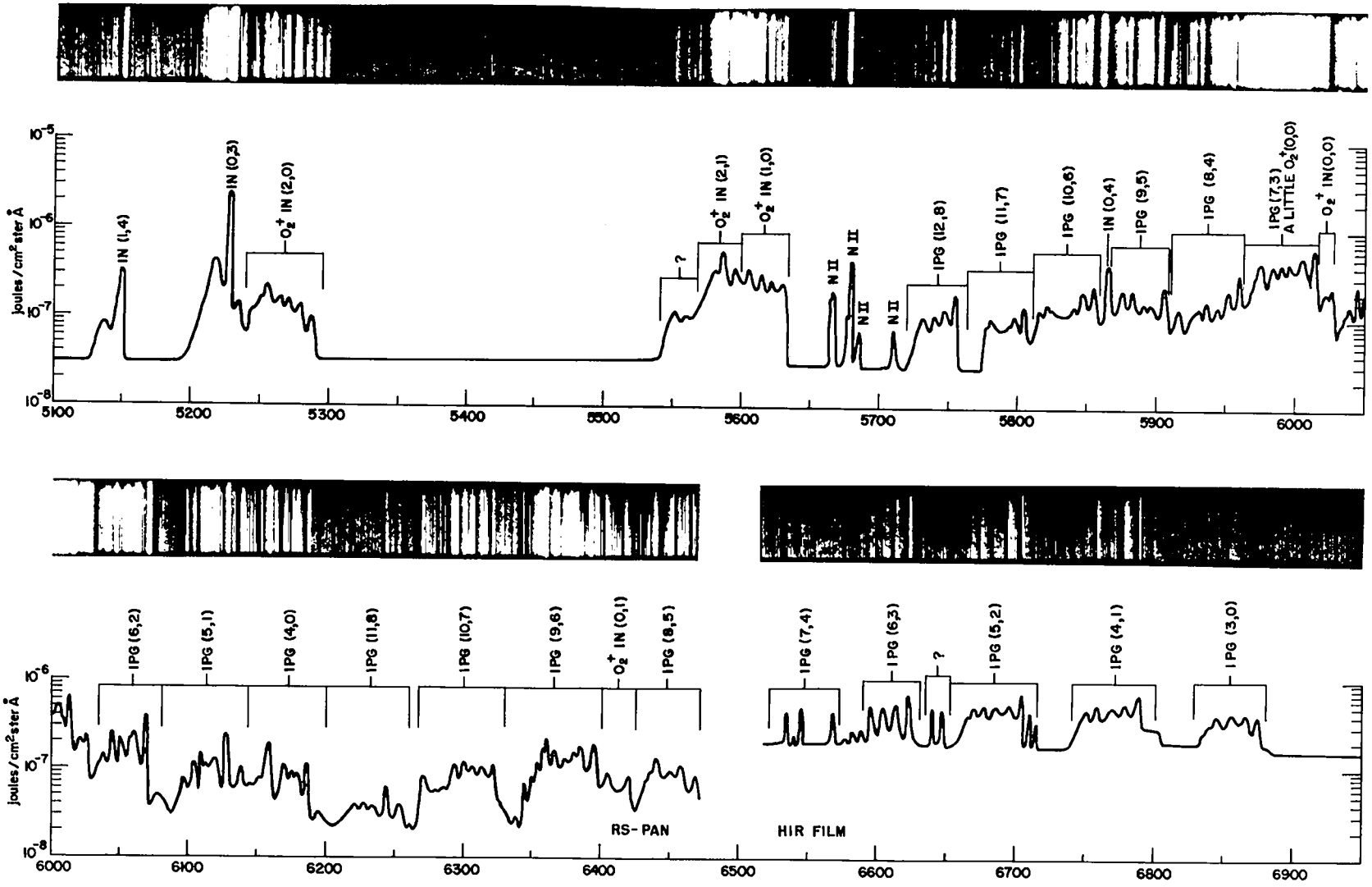

FIG.
X-RAY EXCITED AIR FLUORESCENCE (continued)

Fig. 5. (Continued) 6900 - 8500 Å.

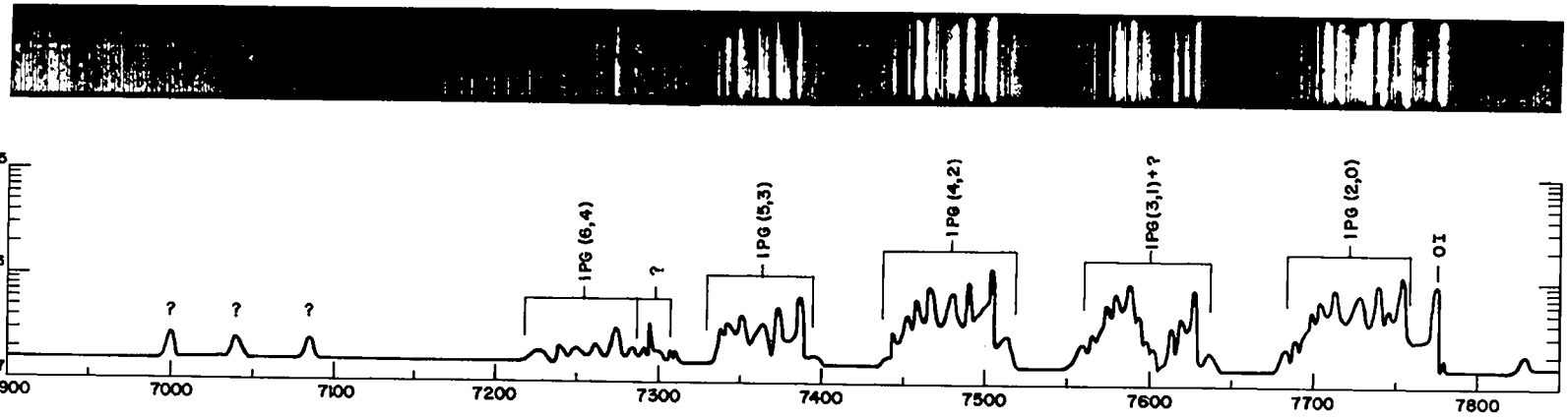

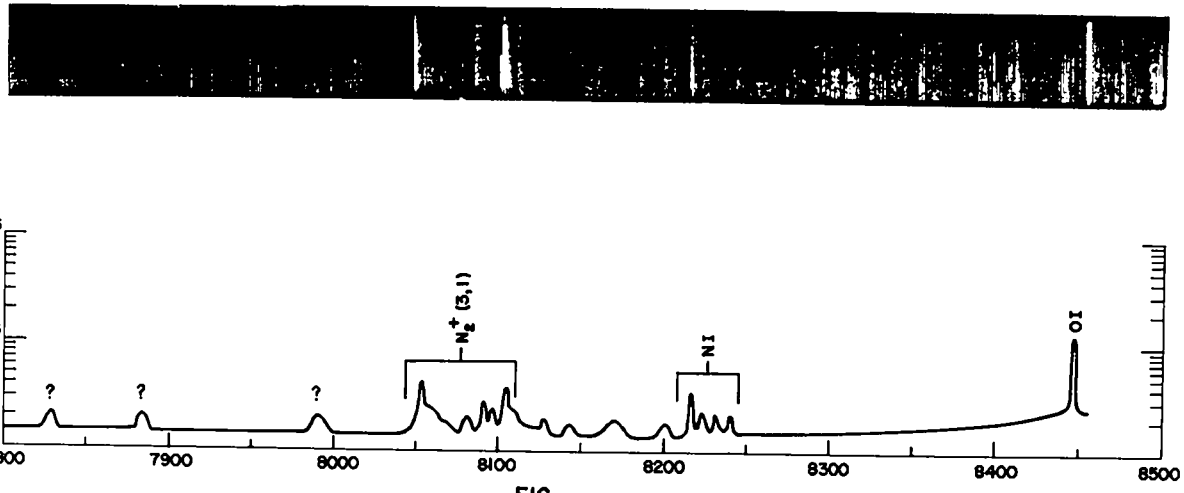

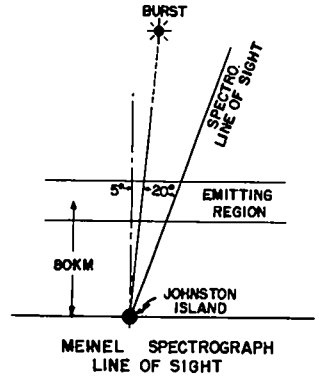

FIG.
X-RAY EXCITED AIR FLUORESCENCE (continued)

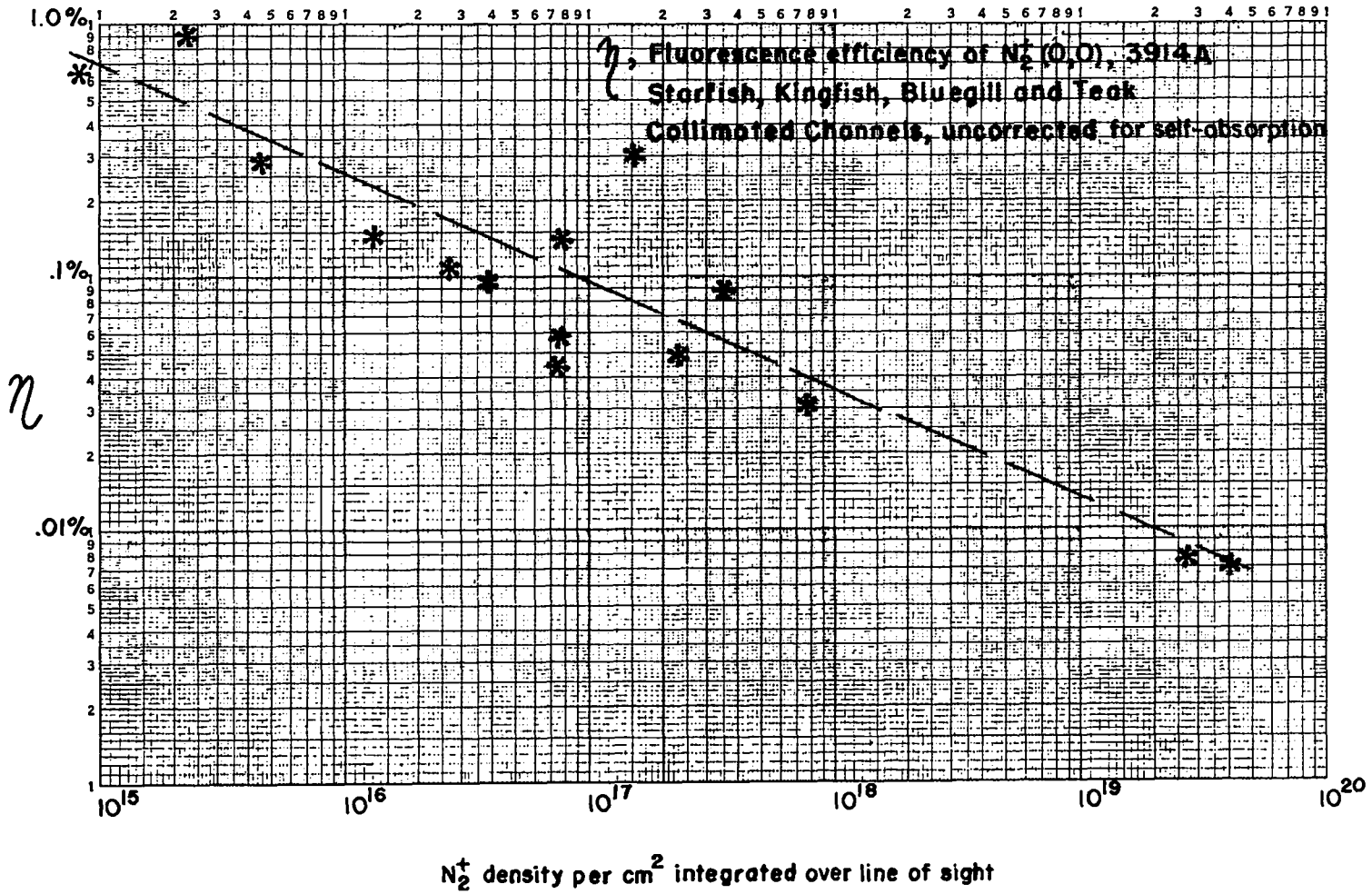
η, Fluorescence efficiency of N_2^+ (0,0), 3914 A
Starfish, Kingfish, Bluegill and Teak
Collimated Channels, uncorrected for self-absorption
1.0%
.1%
.01%
η
10^{15}
10^{16}
10^{17}
10^{18}
10^{19}
10^{20}
N_2^+ density per cm^2 integrated over line of sight

Fig. 6

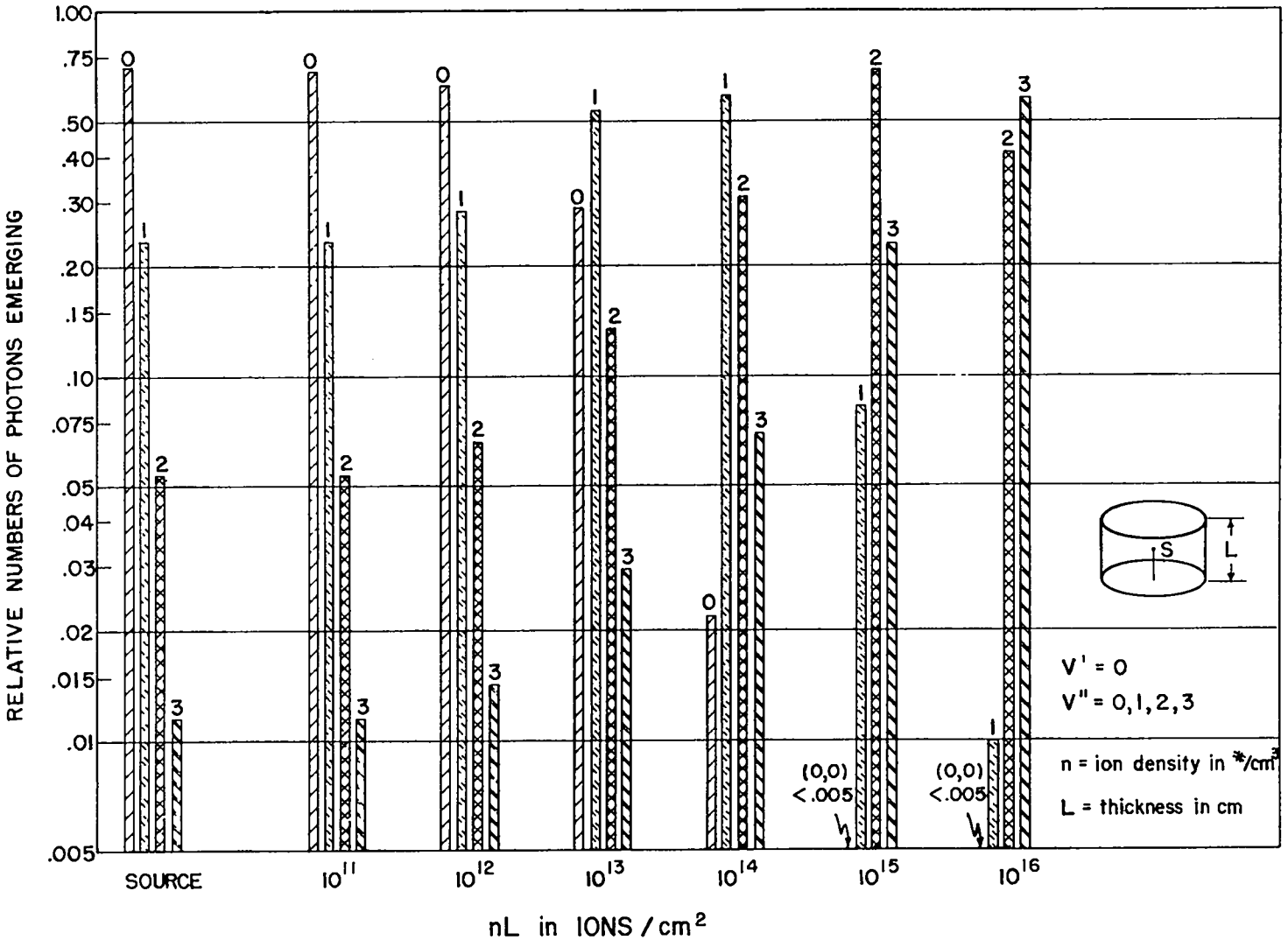

Fig. 7. Types of photons emerging from bottom of cylinder with source located in center.

First Negative System	Rel.Int.Distr. Einstein Coeff. sec^{-1}	Fractional Populations	Effective Absorption Cross Sections cm^2/air ion
3914Å (0,0)	1.07×10^{7}	.872	2.5×10^{-15}
4278Å (0,1)	$.35 \times 10^{7}$	.108	1.3×10^{-16}
4709Å (0,2)	$.08 \times 10^{7}$	.015	5.5×10^{-18}
5228Å (0,3)	$.002 \times 10^{7}$	.003	2.6×10^{-19}

N_2^+ Removal Rates:

Charge exchange with O_2: $\alpha = 2 \times 10^{-10}$ cm^3/sec

Dissociative recombination: $\alpha = 2 \times 10^{-7}$ cm^3/sec

Fig. 8. Source function and basic parameters of random walk - imprisonment calculations for N_2^+, 1N.

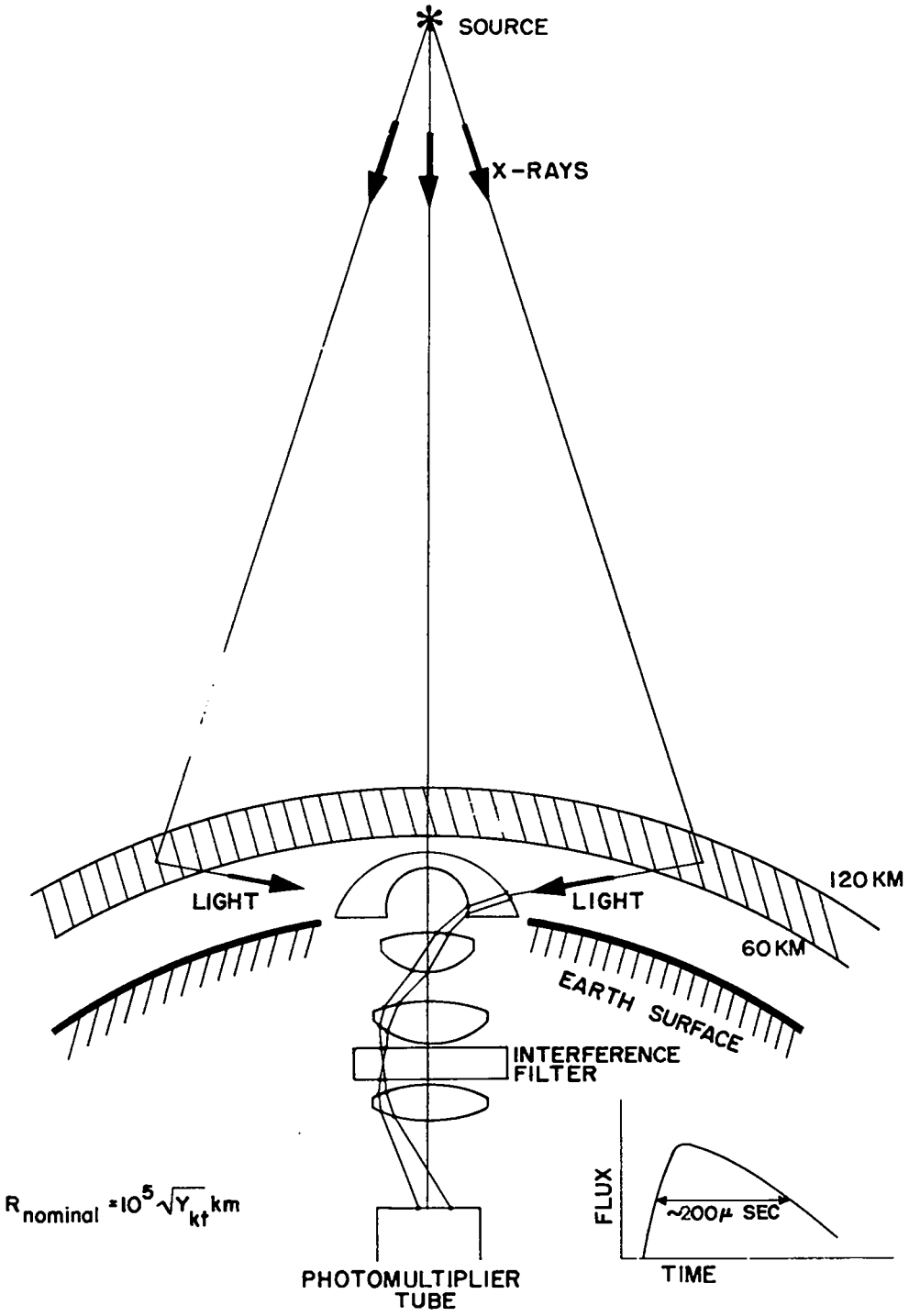

Fig. 9. Vela Sierra detection system (schematic).

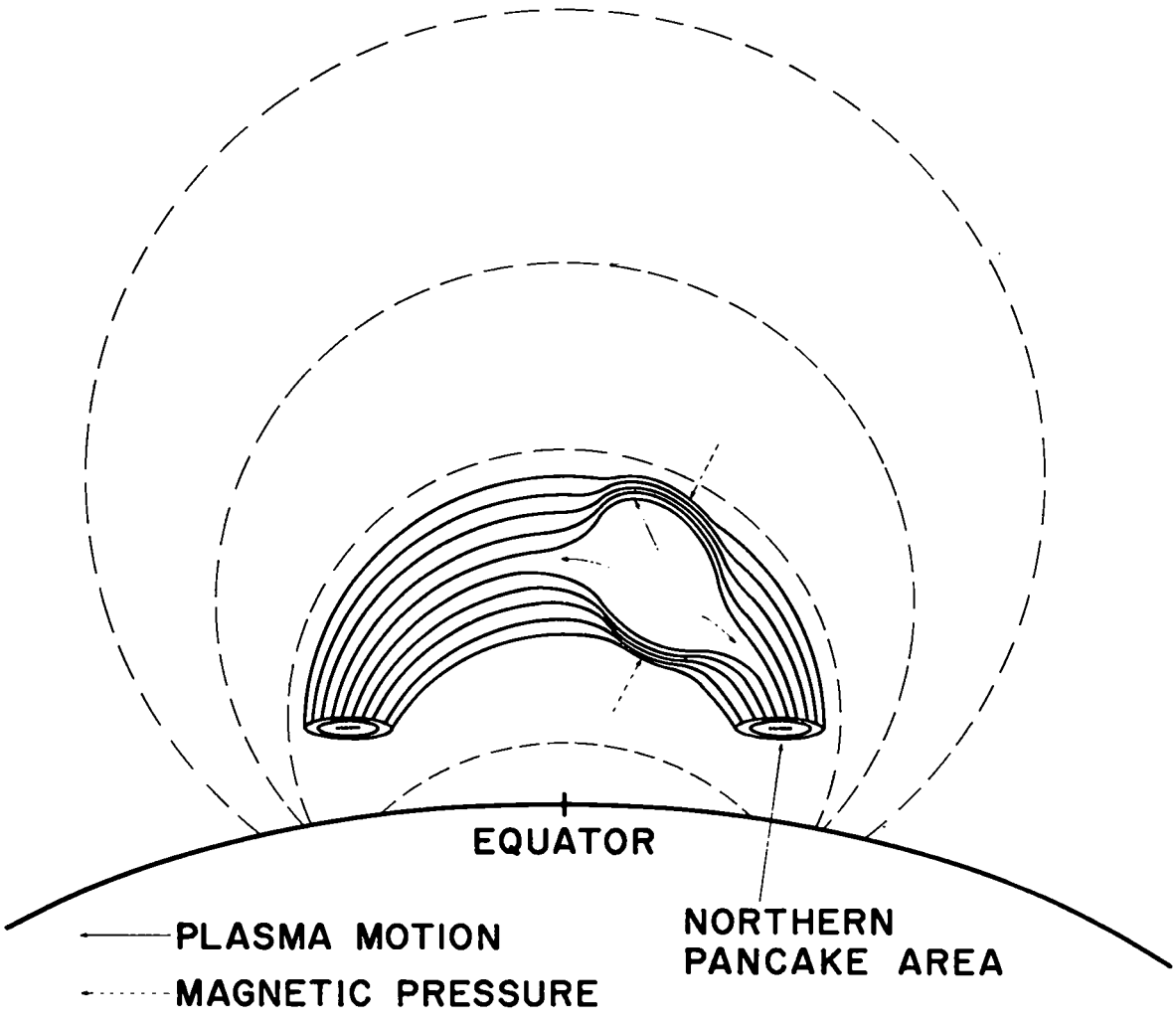

Fig. 10. Early phase of formation of plasma bubble in geomagnetic field (schematic).

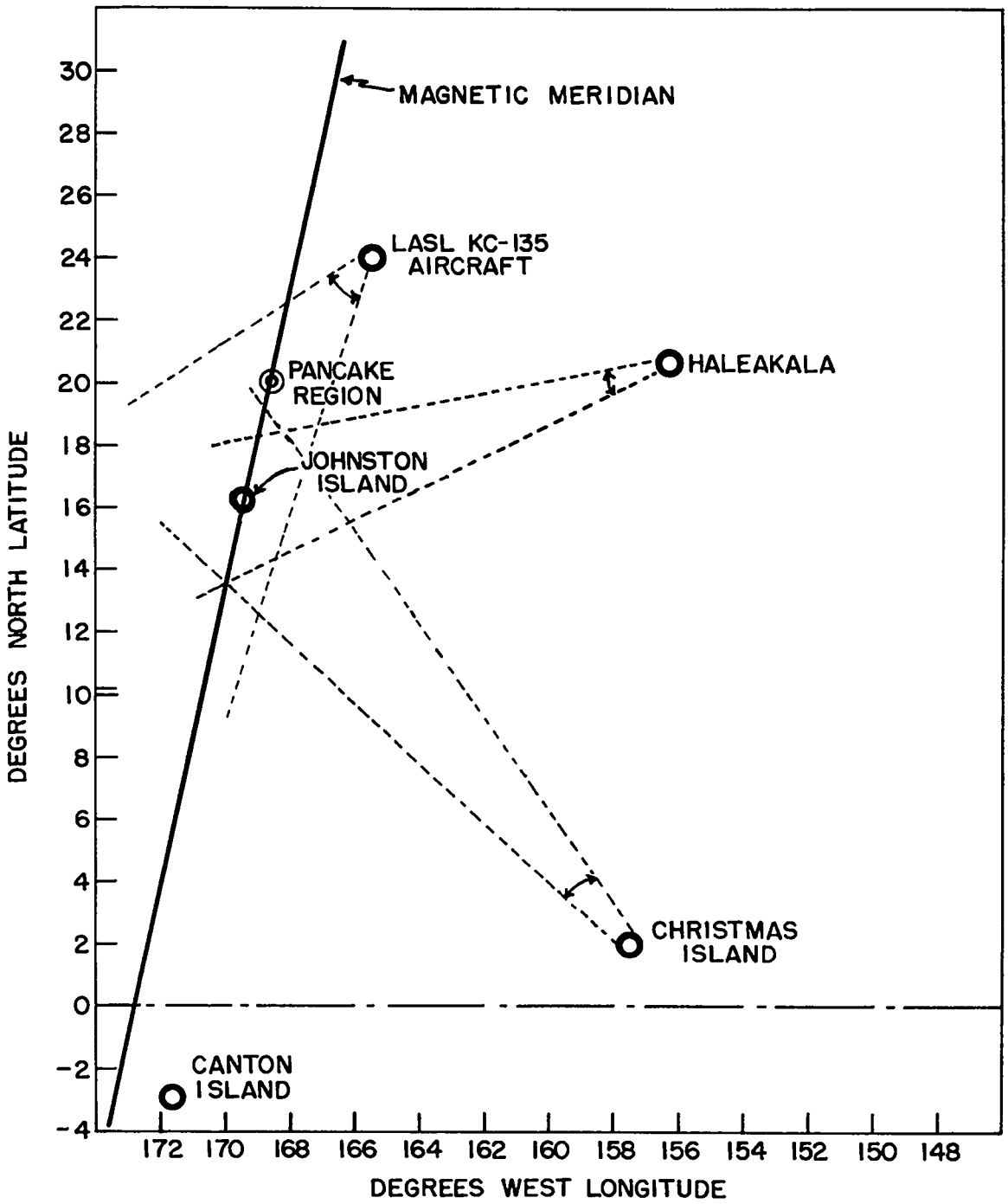

Fig. 11. Sketch of station locations.

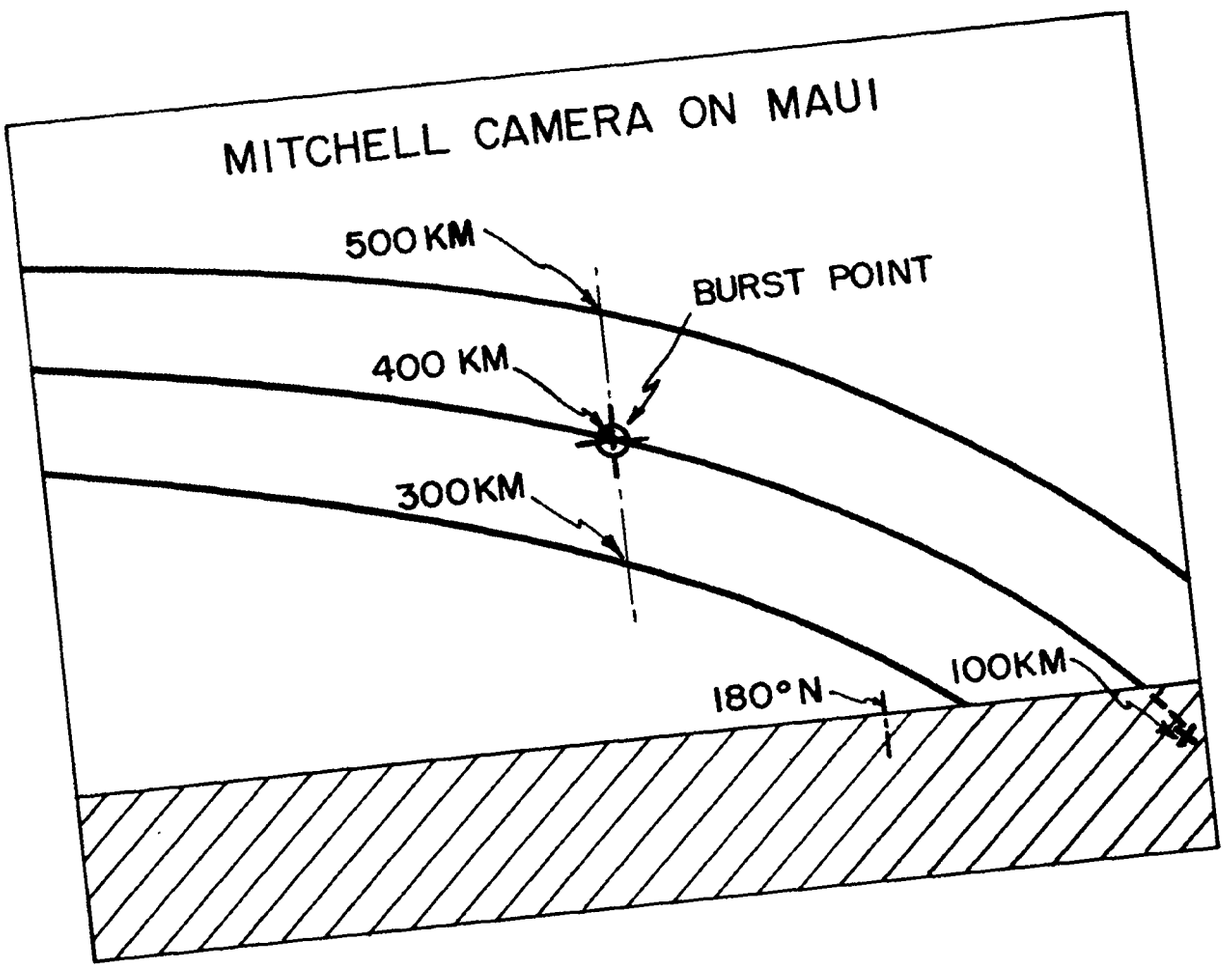

Fig. 12. Projections of geomagnetic field lines into field of view of camera.

Fig. 13. View of burst area, bright booster, "magnetic bubble," and air excited by escaping debris and beta rays to the north (right) from Mt. Haleakala.

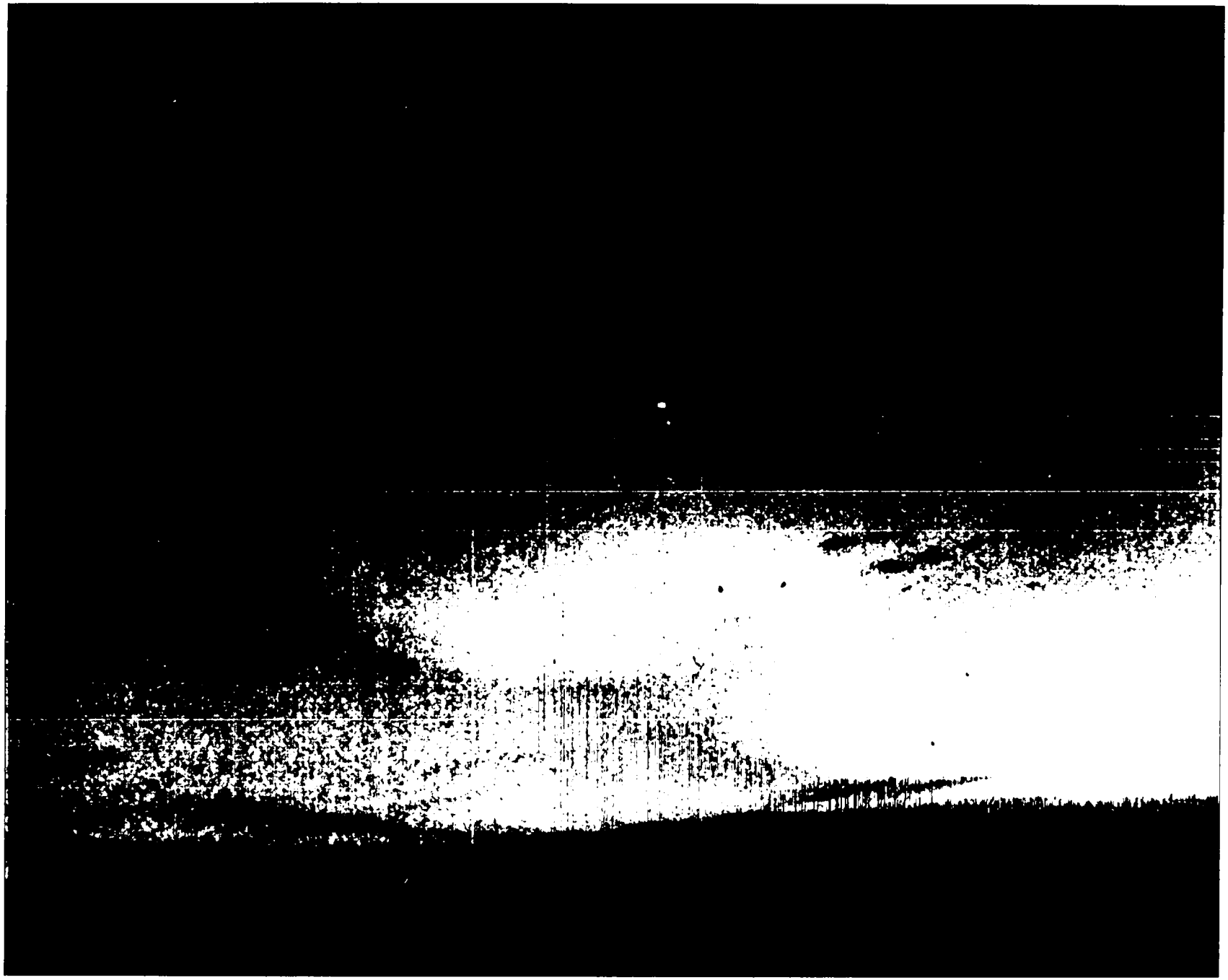

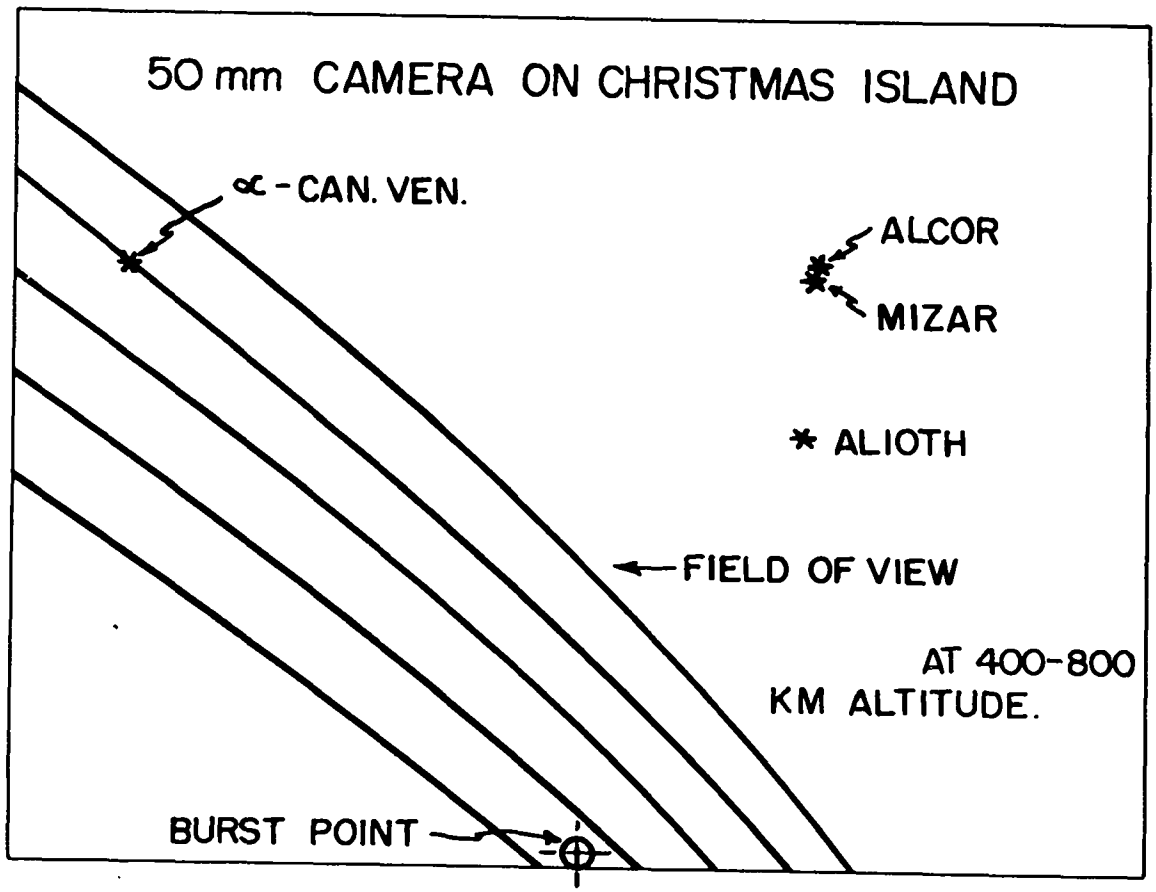

Fig. 14. Projection of magnetic field lines into field of view of camera located on Christmas Island.

Fig. 15. Motion of Starfish debris as seen from Christmas Island at ~ + 1 min.

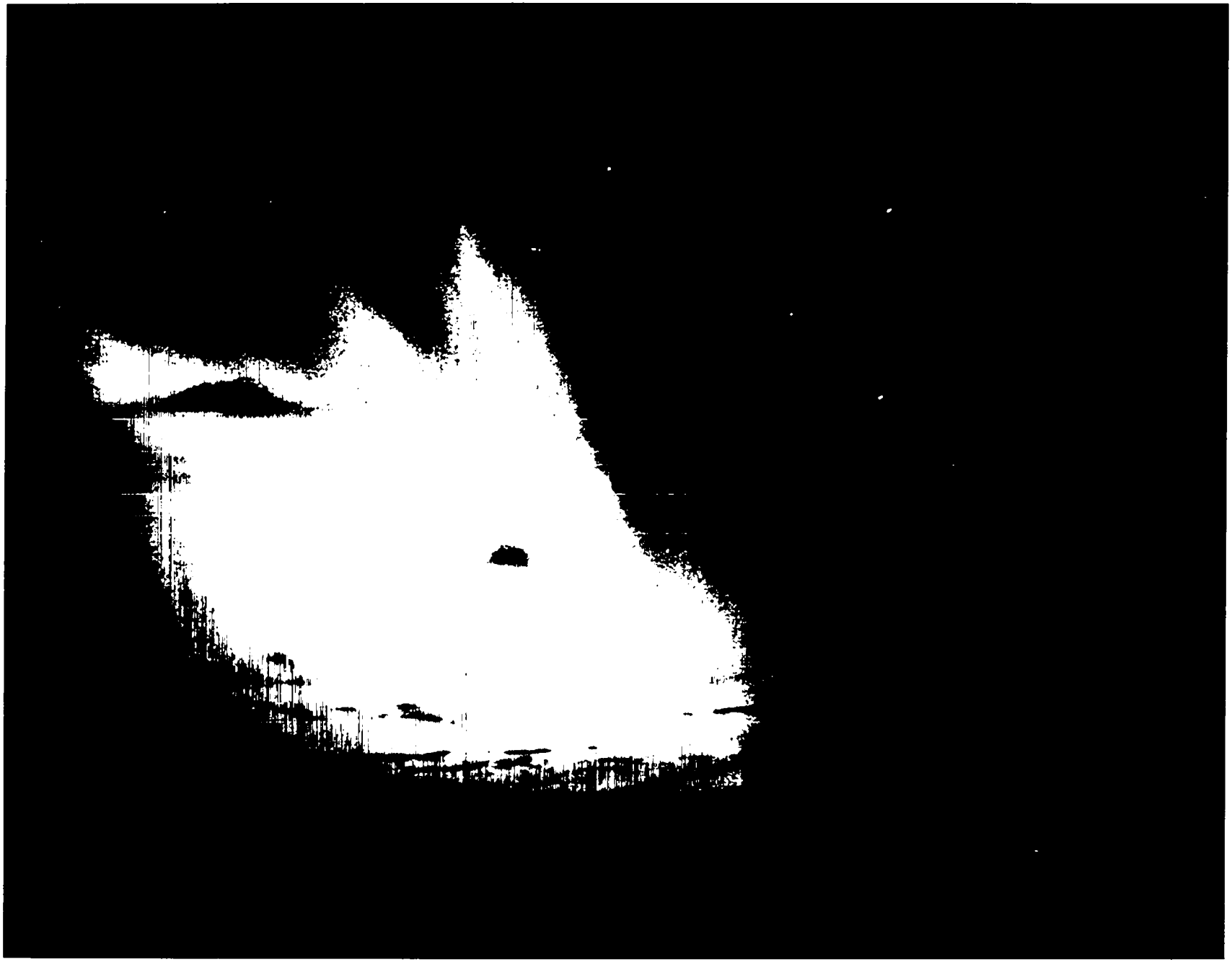

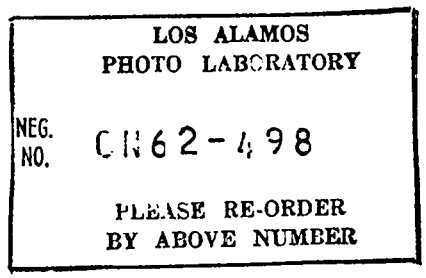
LOS ALAMOS
PHOTO LABORATORY
NEG.
NO. CN62-498
PLEASE RE-ORDER
BY ABOVE NUMBER

Fig. 16. Burst at ~ + 1 min seen from aircraft flying near French Frigate Shoal. Horizontal dimension of field of view at burst distance ~ 1500 km.

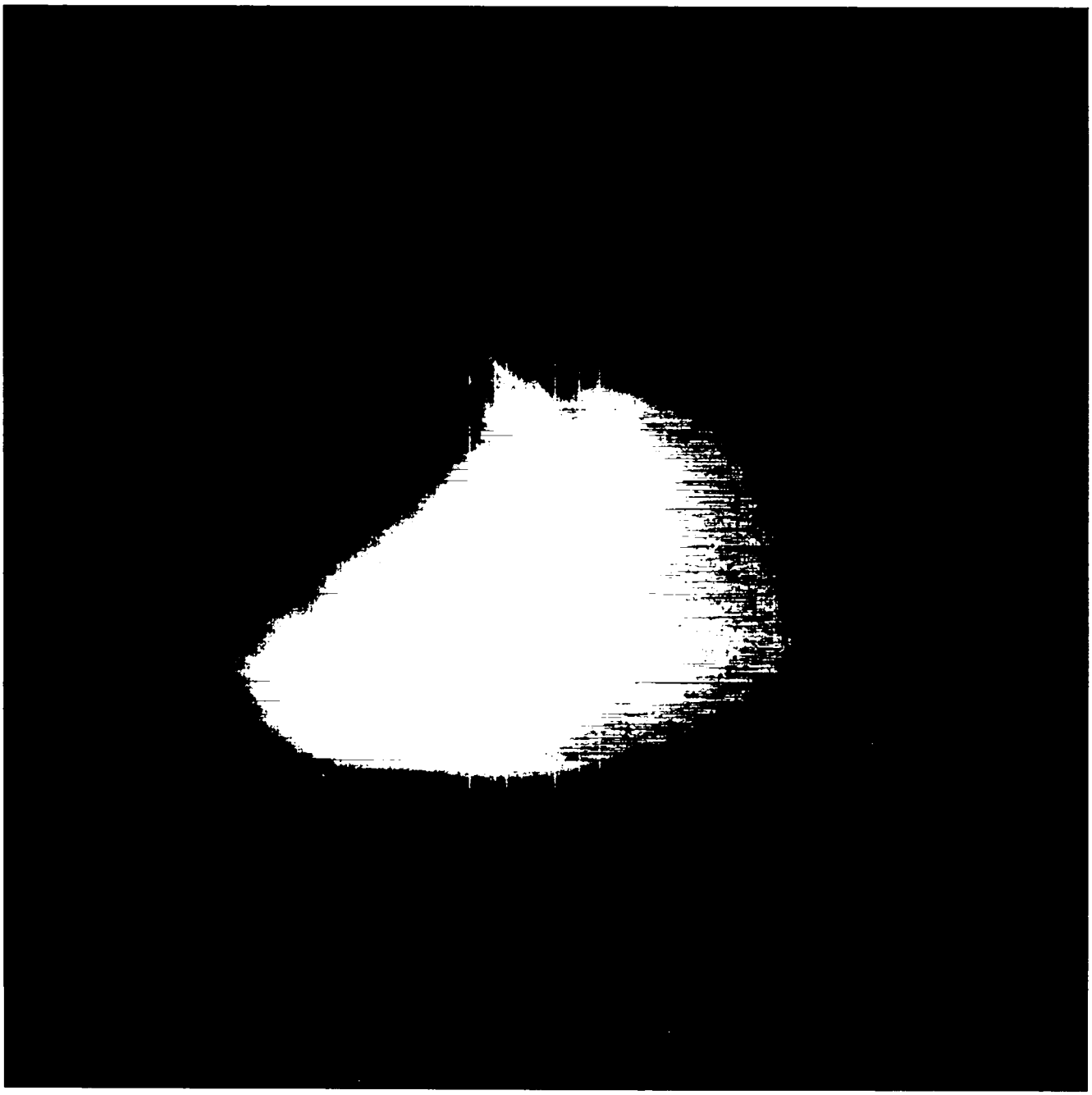

Fig. 17. Debris and shock excited air at + 3 min seen from aircraft. Horizontal dimension of field of view at burst distance ~ 750 km. Compare with projection of field lines in Fig. 18. Note slightly blurred star images. Exposure time 3 sec.

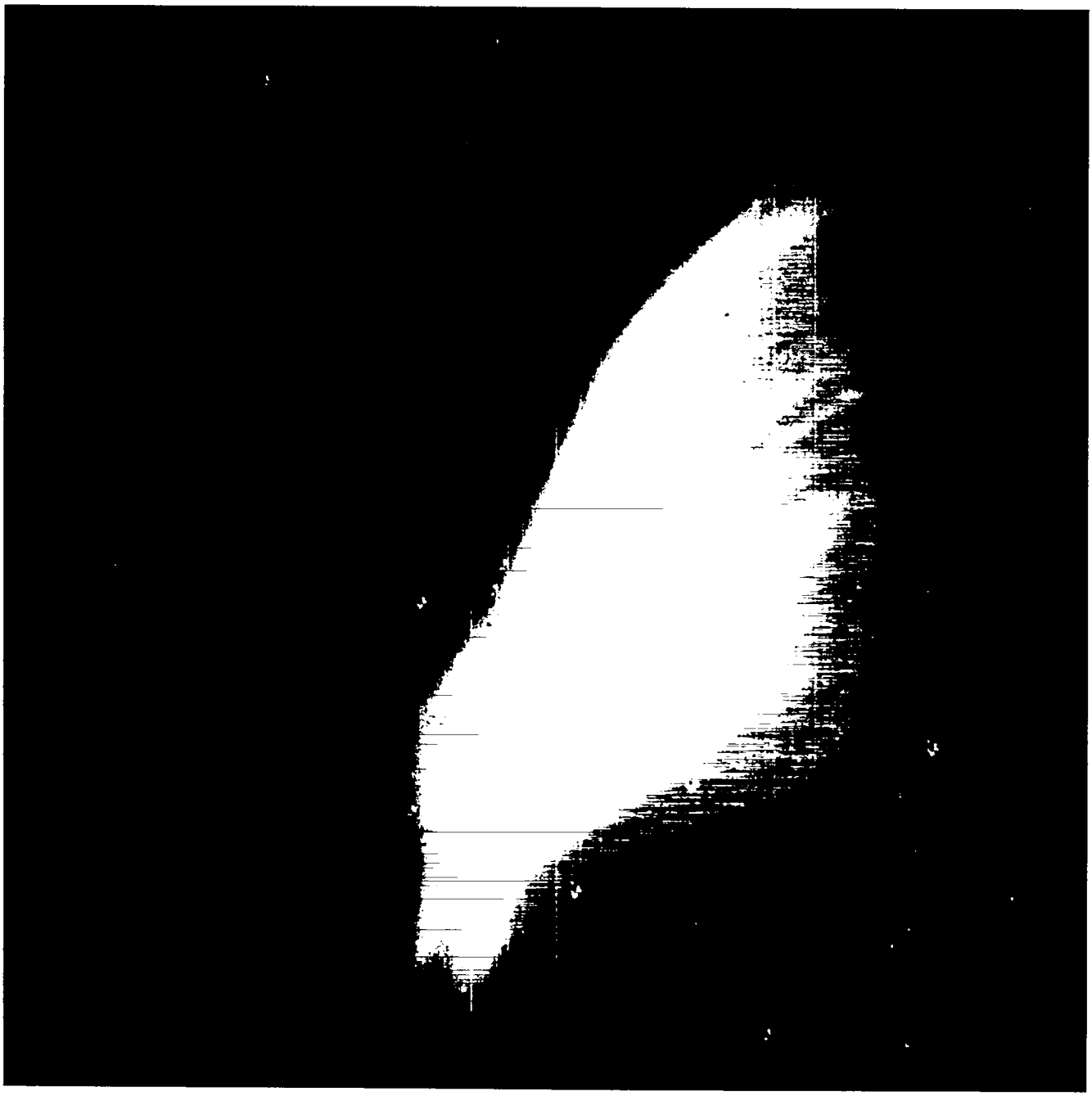

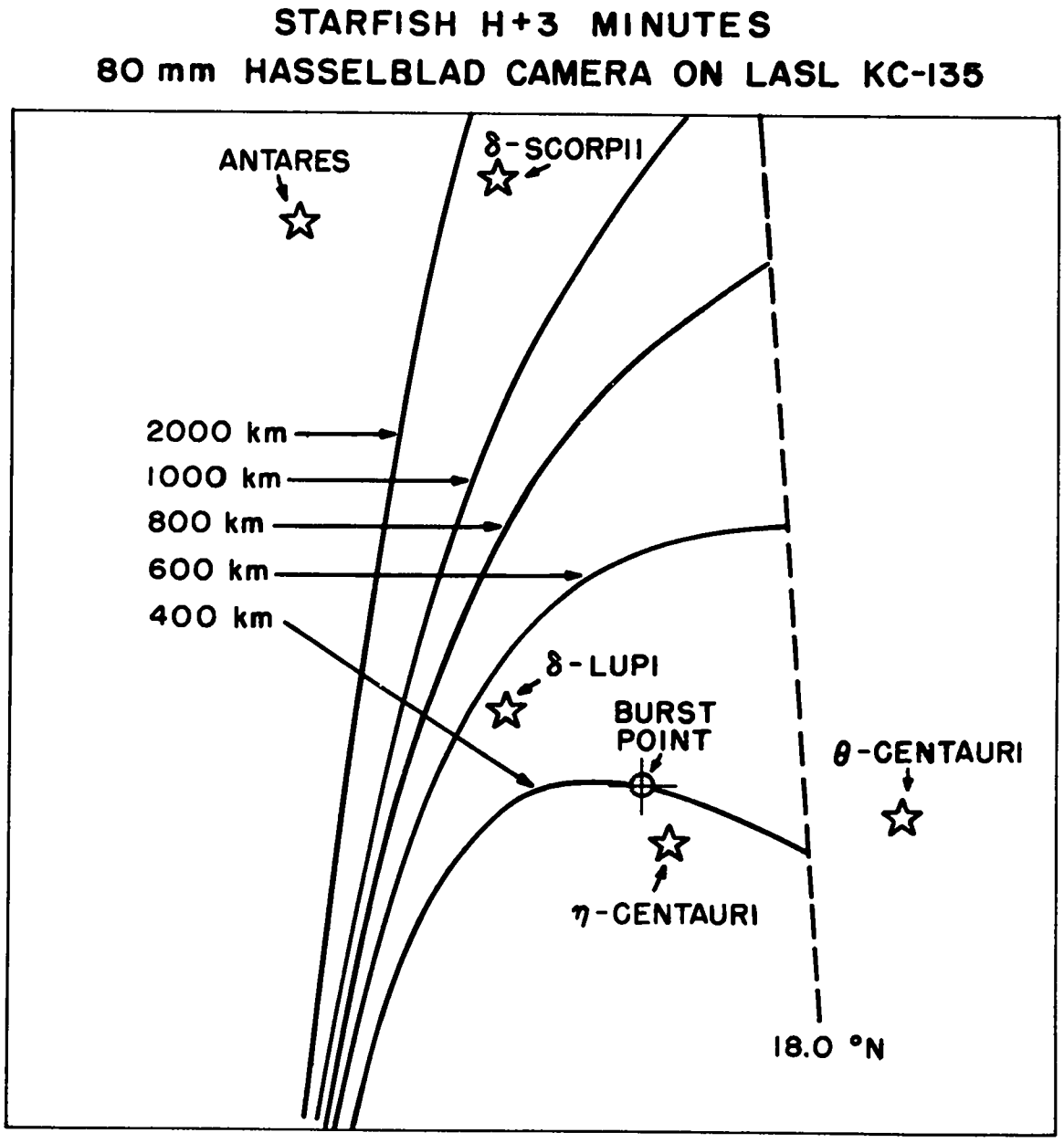

Fig. 18. Projection of geomagnetic field lines into field of view of camera. Compare with Fig. 17.

Fig. 19. Spectrogram of debris streamer taken from aircraft carrier near Johnston Island.

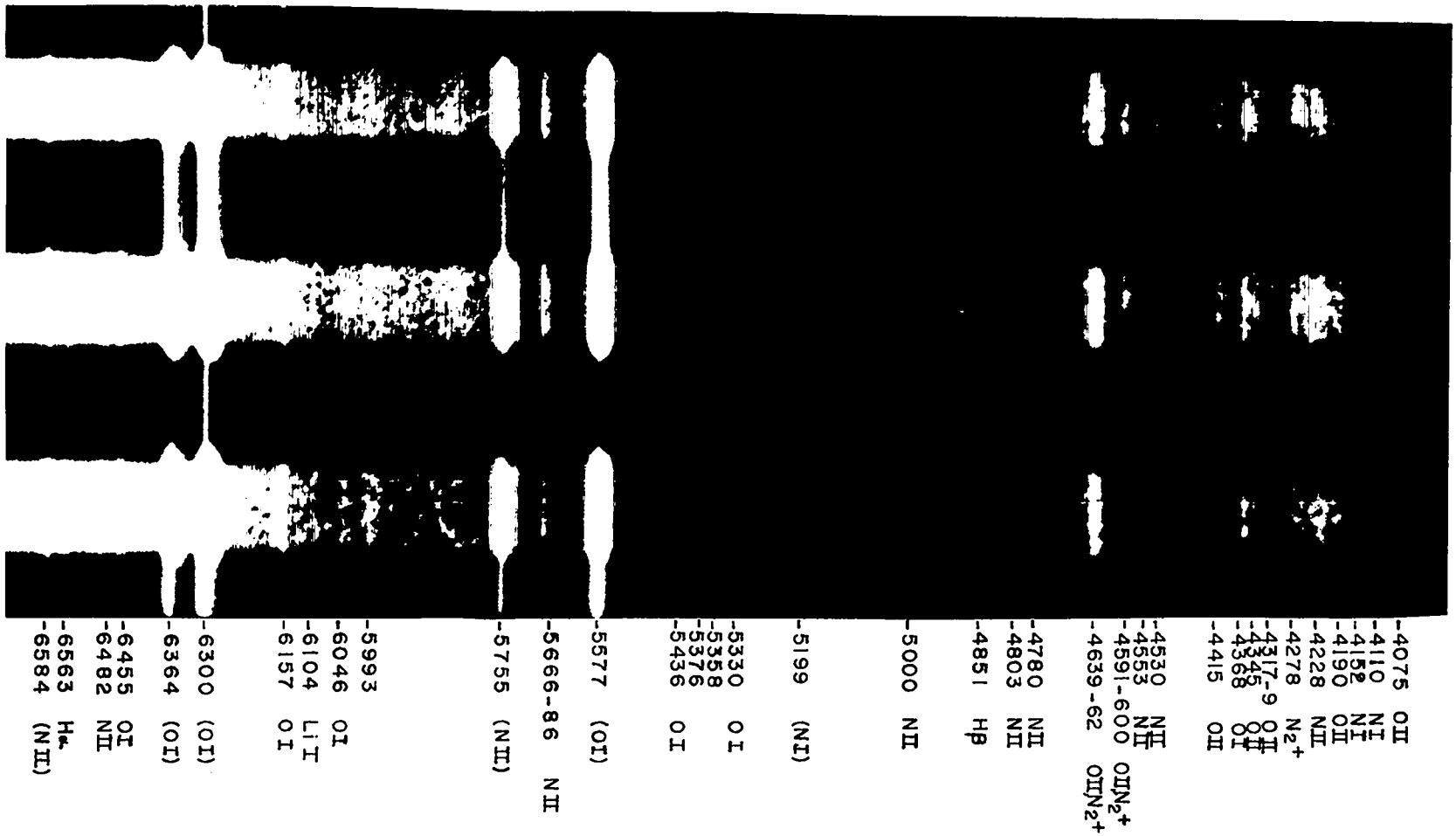

AURORAL SPECTROGRAPH FROM U.S.S. IWO JIMA; Az 12°, El 45° +35-50 seconds